

## General Disclaimer

### One or more of the Following Statements may affect this Document

- This document has been reproduced from the best copy furnished by the organizational source. It is being released in the interest of making available as much information as possible.
- This document may contain data, which exceeds the sheet parameters. It was furnished in this condition by the organizational source and is the best copy available.
- This document may contain tone-on-tone or color graphs, charts and/or pictures, which have been reproduced in black and white.
- This document is paginated as submitted by the original source.
- Portions of this document are not fully legible due to the historical nature of some of the material. However, it is the best reproduction available from the original submission.

STUDIES OF THE CRYSTALLIZATION PROCESS OF ALUM-  
INUM-SILICON ALLOYS USING A HIGH TEMPERATURE  
MICROSCOPE

(NASA-TM-77869) STUDIES OF THE  
CRYSTALLIZATION PROCESS OF ALUMINUM-SILICON  
ALLOYS USING A HIGH TEMPERATURE MICROSCOPE  
Thesis (National Aeronautics and Space  
Administration) 67 p HC A04/MF A01 CSCL 11F G3/26

N85-35272

Unclas  
22235

Stefan Justi

Translation of "Untersuchungen des Kristallisation-  
sablaufs von Aluminium-Silizium-Legierungen im Hoch-  
temperaturmikroskop (mit ergänzenden Beobachtungen an  
eutektischen Silber-Kupfer-, Silber-Silizium-und Gold-  
Silizium-Legierungen)", Technische Universitaet Berlin,  
West Germany, Materials Science Department, Thesis, Aug. 2,  
1971, pages 1-76.



ORIGINAL PAGE IS  
OF POOR QUALITY

STANDARD TITLE PAGE

1. Report No. NASA TM-77869	2. Government Accession No.	3. Recipient's Catalog No.	
4. Title and Subtitle STUDIES OF THE CRYSTALLIZATION PROCESS OF ALUMINUM-SILICON ALLOYS USING A HIGH TEMPERATURE MICROSCOPE		5. Report Date September, 1985	6. Performing Organization Code
		8. Performing Organization Report No.	10. Work Unit No.
7. Author(s)  Stefan Justi		11. Contract or Grant No. NASA- 4004	
		12. Type of Report and Period Covered Translation	
9. Performing Organization Name and Address SCITRAN Box 5456 Santa Barbara, CA 93108		14. Sponsoring Agency Code	
13. Sponsoring Agency Name and Address National Aeronautics and Space Administration Washington, D.C. 20546		15. Supplementary Notes  Translation of "Untersuchungen des Kristallisationsablaufs von Aluminium-Silizium-Legierungen im Hochtemperaturmikroskop (mit ergänzenden Beobachtungen an eutektischen Silber-Kupfer-, Silber-Silizium-und Gold-Silizium-Legierungen)", Technische Univeristaet Berlin, West Germany, Materials Science Department, August 2, 1971, pages 1-76. (N72-20488)	
16. Abstract  It is shown that primary silicon crystals grow polyhedral in super-eutectic AlSi melts and that phosphorus additives to the melt confirm the strong seeding capacity. Primary silicon exhibits stong dendritic seeding effects in eutectic silicon phases of various silicon alloys, whereas primary aluminum does not possess this capacity. Sodium addition also produces a dendritic silicon network growth in the interior of the sample that is attributed to the slower silicon diffusion velocity during cooling.			
17. Key Words (Selected by Author(s))		18. Distribution Statement  Unclassified and Unlimited	
19. Security Classif. (of this report) Unclassified	20. Security Classif. (of this page) Unclassified	21. No. of Pages 65	22. Price

## TABLE OF CONTENTS

1. Introduction	3
2. Short summary about the high temperature microscope in metal sciences	5
3. Previous analyses of Al-Si alloys	8
3.1 The phase diagram	8
3.2 Morphology of the primary crystallization phases	9
3.21 Al as the primary crystallization phase	9
3.22 Si as the primary crystallization phase	9
3.3 Morphology of the eutectic	10
3.31 Subordination of the eutectic	10
3.32 Directed solidification	13
3.33 Matrix formation with increased cooling rate	16
3.34 Nucleus formation	17
3.4 Enriching	17
3.41 Formation of the $\text{NaAlSi}_4$ phase	18
3.42 Growth inhibition	18
3.43 Inhibition of the nucleus formation of the silicon	19
4. Tests	21
4.1 Test plan	21
4.2 Production of sample materials	21
4.3 Test description	22
5. Test results	28
5.1 Al-Si 18	28
5.2 Al-Si alloy	29
5.21 Al-Si 18	29
5.22 Adding of phosphorus to the AlSi 18-melting	30
5.23 AlSi 12.5	30
5.24 AlSi 6	32
5.25 Crystallization rate	33
5.26 The interdendritic interval	33
5.27 Adding of sodium to the AlSi 12.5 melting	34
5.28 Raster scan electron microscopic photographs	36
5.4 AuSi 4 alloy	37
6. Discussion of the test results	37
7. Summary	43



8.	Photo part	44
8.0	Eutectic crystallization of the AgCu alloy	45
8.1	Crystallization of the AlSi 18 alloy	46
8.2	Crystallization of the AlSi alloy	48
8.3	Eutectic crystallization of the alloy AlSi 12.5	50
8.4	Eutectic crystallization of the AlSi 12.5 alloy	52
8.5	Crystallization of the AlSi 6 alloy without temperature measurement	54
8.6	Eutectic crystallization of the AlSi 12.5 alloy	55
8.7	Grid scan electron microscopic photographs	56
8.8	Eutectic crystallization of the AgSi 3.6 alloy	58
8.9	Eutectic crystallization of the AuSi 4 alloy	59
	References	60

STUDIES OF THE CRYSTALLIZATION PROCESS OF ALUMINUM-SILICON  
ALLOYS USING A HIGH TEMPERATURE MICROSCOPE

Stefan Justi

1. Introduction

\*5

Alloys of aluminum and silicon have been used as materials for pistons and motor housings. Essential for this are some desirable physical and technological characteristics, such as, i.e., the high thermal conductivity, whereby local temperature peaks can be rapidly transferred to a cooling medium, in addition to a low price. The good capacity for mold filling and flow of the alloy during the casting is of great importance, since the motor housings and pistons usually have a complicated geometric structure. It can be easily seen that a perfect thin-walled casting makes difficult and expensive mechanical processing unnecessary. The relatively low casting temperature is another advantage, since the eutectic temperature is  $T = 577^{\circ}\text{C}$ .

These advantages offset the unfavorable aspects of mechanical properties, strength and durability. The elongated silicon needles or lamella form in the matrix of high purity Al-Si alloys, and a number that are ray-shaped are imbedded in the Al-matrix (lamella, silicon, photo 1.1).

The alloys of lower purity that can be achieved in practice exhibit a matrix which exudes coarse and irregular eutectic silicon in needle shape and sometimes in the shape of polyhedral crystals (crystallized silumin, photo 1.2). Tension peaks develop on these needles with mechanical stress which represent the cause of a low yield strength and breaking tension. A considerable improvement in the mechanical characteristics is achieved through

---

\* Numbers in margin indicate pagination of foreign text.

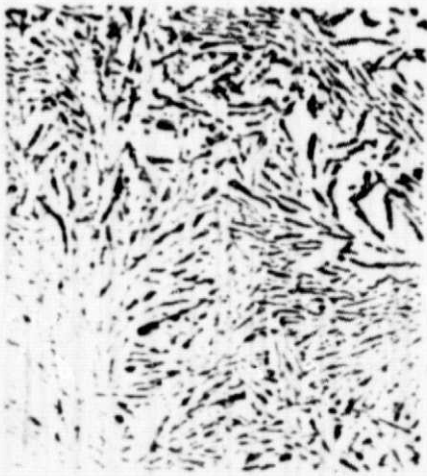


Photo 1.1: Lamella



Photo 1.2: Granular

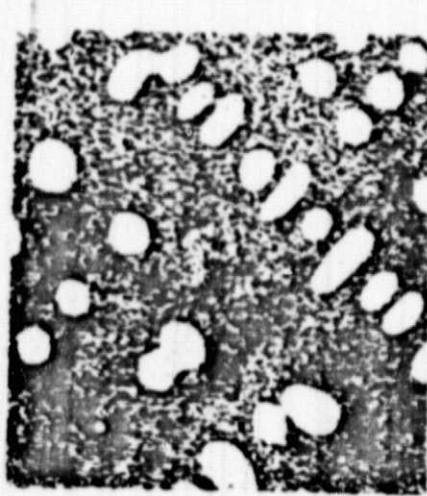


Photo 1.3: Enriched AlSi-Eutectic



Photo 1.4: Overeutectic Al-Si-alloy, without phosphorus

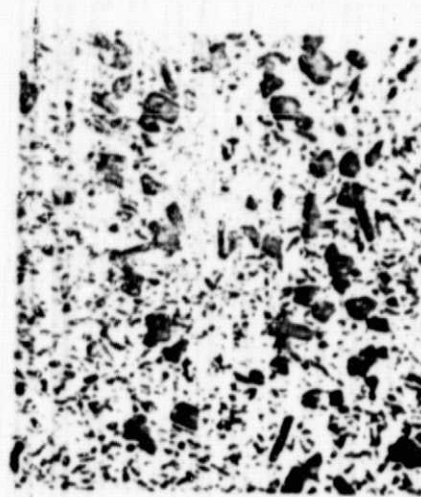


Photo 1.5: Overeutectic Al-Si alloy, with phosphorus

Scale:

Photo 1.1

1.2 ——— = 100 μm

1.3

Photo 1.4 ——— = 100 μm

1.5

The photos were extracted from a study by K. Löhnberg [1]

ORIGINAL PAGE IS OF POOR QUALITY

the treating of the melting with sodium which is added in metallic or salt form before the casting. The eutectic silicon is now exuded in the form of small round crystals. The process is called "enrichment" (photo 1.3).

In the case of overeutectic Al-Si alloys that are characterized by a higher resistance to wear compared to the undereutectic alloys, but with a reduced thermal conductance, primary silicon develops in the shape of very coarse and fissured sheets (photo 1.4). With a small addition of phosphorus, the primary silicon is exuded in the form of many small polyhedral crystals (photo 1.5). Technical use is made of the possibility of this "fine crystal".

The objective of this study is to follow the crystallization process in Al-Si alloys using a high temperature microscope, and to attempt to evaluate the sodium enrichment with the diffusion, surface tension and wetting angle measurements of Korber [2].

## 2. Short summary about the high temperature microscope in metal sciences

/8

Since the first hot-table microscope matrix tests by P. Oberhoffer [3] in 1909, high temperature microscopy has developed into a metal sciences testing method which, due to the capability of detecting certain processes immediately and due to its high clarity, has continually gained in importance. In [4-6], there are detailed examples of the many possible applications of high temperature microscopy.

The subsequent chapter deals with the dissertation by Schneider [7] which also contains extensive references to other reference sources.

In examining metals and metal alloys in a high temperature microscope, they must distinguish between the tests of matrix changes in the fixed state and the tests of the melting and solidification processes.

In the former, the matrix changes of steel in the cooling from the austenite range were of interest. High temperature microscopy has contributed much to the clarification of the formation and growth mechanism of the martensite.

These matrix changes of steels (i.e., martensite, intermediate stages and perlite formation) associated with the volume changes as well as extrusion (i.e., formation of temper carbons) are associated with a relief formation and contrast changes to the picture. They can be immediately perceived in contrast to the crystal limits which first become visible with "thermic etching". Tests have been carried out on the crystal growth and crystal size at high temperatures on the heating table on steel and nonferrous metals, whereby the tests on the recrystallization of nonferrous metals [8], zinc [9,10] and beryllium [11] should be mentioned.

Allotropic matrix changes of pure metals and metal alloys are the subjects of numerous publications.

/9

The tests on the heating table on zinc and platinum with tension stress at high temperatures are also of interest [10,12].

The observation of the melt and solidification processes of metallic materials under the high temperature microscope are very extensive. The location of the melting as well as the exact melting and solidification temperatures were able to be determined for iron and nonferrous metals. The starting of the melting of continuous casting ingots of pure aluminum and refinings in the segregation zones [13], the start of melt of tin, antimony-alloys [14], observations of silver, cadmium-bismuth and copper-nickel alloys [15], of pure zinc [16,10], ruthenium with

1% silicon [8], nickel [17] and unknown systems of the platinum metals [18-20] were the subject of publications. For this study, the observations of the melt of an Al-Si alloy by Jeglitsch [21] are of special interest.

Turnbull and Cech [23-25] were able to show, with the help of heating table microscopic tests on metal meltings and a copper-nickel alloy, that the maximum undercooling in very pure metal melts can amount to up to  $0.18 \cdot T_s$  ( $T_s$  = absolute melting temperature). Of the numerous works on pure iron, steel and casting iron, only the works by Schneider [7] will be mentioned here to remain with the scope of this study.

The question of to what extent the nucleus formation and growth processes are influenced during phase conversions, exudation and crystallization processes by the various energy conditions on the surface and in the interior of the sample has repeatedly arisen. Various nucleus formation conditions could lead to matrix changes on the surface and internally. They have often been given as the reason for the appearance of matrix components which could not be explained by the present equilibrium diagram. At present, it can also not be shown that processes which are associated with a volume enlargement initiate more rapid processes due to the lower pressure on the surface compared to the interior of the sample, and thus could lead to different growth conditions.

/10

In the case of alloy components with very different densities, in spite of the very small melting amounts used with the heating table, it can nevertheless lead to difficulties whereby a completely different crystallization picture results on the surface than in the interior [26]. Finally, the possibility must be considered that the selective evaporation of alloy elements and the associated change in the chemical composition on the surface of the sample can also lead to different processes on the surface and

in the interior. This increasing influence with increasing temperatures and test times in the vacuum can be sharply limited or even prevented through the utilization of inert gases [27].

An oxidation of the sample surface and a change to the energy conditions associated with it cannot itself be fully avoided in the vacuum of  $10^{-6}$  to  $10^{-7}$  torr or with the use of the purest inert gas [28,29], since the partial pressure of the oxygen is still a power of 10 above the equilibrium pressure of many oxides even in these vacuums [30,31]. It can be determined, however, that the amount of oxide is so small that it lays as thin transparent film on the surface of the sample.

In the use of the heating table microscope, it must be very critically considered whether the action on the surface of the sample is representative of the action in the interior of the sample. In any case, other methods of analysis should also be used, i.e., the metallographic microsection, a staged removal of the material from the upper surface or the chemical elimination of certain phases.

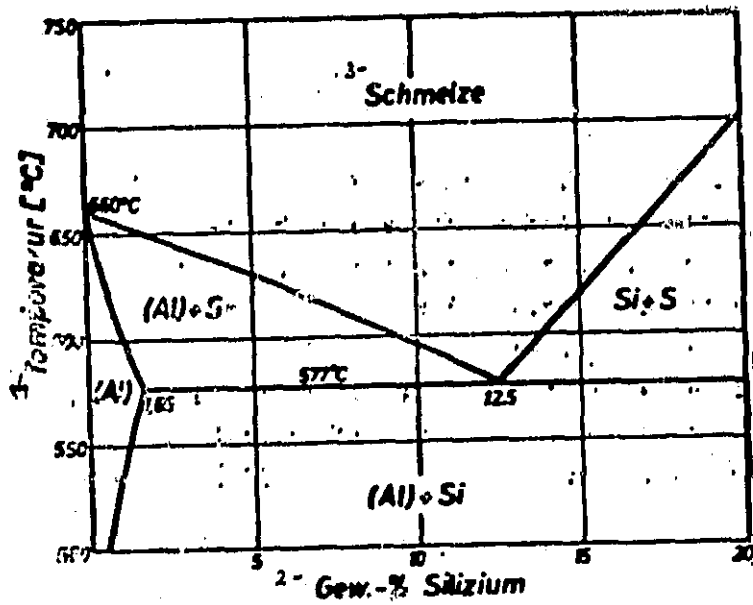
The heating table microscope is very suitable for research on formation and growth mechanisms, but, in quantitative analyses with the help of the heating table microscope alone, caution is advised due to the special conditions on the surface.

### 3. Previous analyses of Al-Si alloys

/11

#### 3.1 The phase diagram

Aluminum and silicon form a eutectic with a presently insured concentration of 1.5% by weight silicon and a temperature of 577°C. Silicon is dissolvable in aluminum up to 1.65% by weight, while aluminum is indissolvable or nearly indissolvable in silicon (Figure 3.1).



ORIGINAL PAGE IS  
OF POOR QUALITY

Figure 3.1: The System Al-Si [32]

1--temperature 2--wt.-% silicon 3--melting

### 3.2 Morphology of the primary crystallization phases

#### 3.2.1 Al as the primary crystallization phase

With slower cooling of an undereutectic Al-Si melt aluminum-enriched mixed crystals form and grow into relatively coarse dendritic structures. An increase in the cooling rate has an effect on the refining of the Al-dendrites.

A treatment of the melt with sodium does not affect the formation of the primary crystals [33], but only the formation the eutectic.

#### 3.2.2 Si as the primary crystallization phase

From overeutectic melting, the silicon crystallized in the form of very coarse fissured sheets with slower cooling which are often star-shaped (photo 1.4). With an increase in the cooling rate, the number of the Si-primary crystals increases, while their size decreases. Some authors observed the crystallization of the primary silicon as dendritic plumed crystals at higher cooling rates [34-39]. A small addition of phosphorus, as is



always the case in technological melt, also leads to a larger number of small polyhedron Si-primary crystals at a slow cooling rate (photo 4.5). Many indications show that P with Al form the compound AlP and, due to the great similarity in the grid structure, the aluminum phosphide works as a foreign nucleus for the crystallization of the silicon [36,40].

A sodium treatment does not only affect the formation of the eutectic, but also causes a rounder solidification of the primary silicon [37-39].

### 3.3 Morphology of the eutectic

It was already mentioned in the introduction that the silicon forms elongated needles or lamellae, from which a number of ray-shaped ones are imbedded in the Al-basic mass as long as the alloy is extensively free of contaminants (photo 1.1).

#### 3.31 Subordination of the eutectic

There is no lack of attempts at classifying binary eutectic systems from various points of view. Chadwick [41] distinguishes between eutectics with a continual and a discontinual structure. The Al-Si eutectic falls in the latter group, since the eutectic silicon phase does not show any connection over a larger area according to his studies.

/13

Scheil [42,43] breaks down the eutectic matrix into normal and abnormal or contaminated. The normal eutectic matrix formation is characterized by the alternating arrangement of the two phases as parallel lamellae, and the formation of a single phase as parallel rodlets in the matrix of the second phase, in case the volume part is predominant.

The individual eutectic crystals are diagonally identifiable. Within a eutectic crystal, the phase of the same type has the same

orientation; it thus represents a monocrystal. The crystallization of the two phases, between which there is an orientation, is closely linked, which means the crystallization of the one phase makes that of the other easier, so that the common crystallization can take place more rapidly than one that is spatially separated. They also speak of a lamella eutectic. Kraft [44] traces this to the efforts of both types of crystals to form a border surface with as little energy as possible. There is, therefore, a common crystallization front.

These do not develop with the abnormal eutectic crystallization. The coupling in the solidification of the two matrix components is no longer so strong or no longer exists. This leads to one of the two phases being able to bring about the crystallization, which no longer runs parallel, but is oriented after the growth laws of the earlier phase. This does not prevent the coupling from being very tight in certain matrix areas. Individual eutectic crystals are not generally diagonally identifiable.

/14

Scheil proposes two quantities for the classification of the eutectics--the volume ratio of the two phases and quotient which consists of the melting temperatures of the two pure components and the temperature of the eutectic.

With the help of these characteristics, Scheil was successful in classifying about 75% of the existing eutectics in a diagram which can be divided into three areas, each with a range for normal and abnormal eutectics as well as a transition range.

The classification has the disadvantage of not being able to distinguish between normal and abnormal eutectic alloys in the transition range.

Davies [45] assumes the diffusion before the lamella peaks as the determining factor for the crystallization speed. With increasing distances of the lamella peaks, the diffusion of the

enriched components in front of the one type of lamella becomes more difficult to the adjacent type of lamella. With sufficiently large intervals in the two lamella peaks, both phases could grow independently from the other, so that an abnormal or completely contaminated matrix develops. The Davies parameter contains the volume ratio and the climb of the liquid lines of the two eutectic phases as well as the width of the lamella. Up to a certain value of the Davies parameter, one gets a normal eutectic and above that an abnormal eutectic.

These attempts to classify the eutectic alloys could not be satisfactory. They basically contained only a matrix description of a two-dimensional micrograph. Kinetic growth values from which conclusions could be drawn on the three-dimensional process of the crystallization were not considered.

Hunt and Jackson [46] select the melting entropy of a material as the classification characteristic. With a low melting entropy, as is the case with metals, the interface between the fluid and solid phase is not very marked. Metalloids and semi-/15conductors, however, have a high melting entropy and a very marked phase interface. The solid phase grows in facets to the liquid phase.

With regard to the formation of the interfaces, Hunt and Jackson divide the binary eutectics into three groups, whereby it is presumed that the phases in the eutectic crystallization will retain their condition in the solidification as if they would expand in their own melting.

1. Both phases have a low melt entropy and do not expand in facet shapes. The result is a lamellate or rod shaped structure of the eutectic. Examples are the systems: Pb-Sn, Cd-Sn, Cd-Pb, Sn-Zn, Al-Zn, Ag-Cu.

2. One of the two phases has a high melt entropy; the other has a low melt entropy. The structures are usually irregular, but sometimes there are regular structures in individual zones, especially if the melting is slightly enriched with the facet-like increasing phase. Examples: Al-Si, Bi-Pb, Bi-Sn, Ag-Si, Au-Si.
3. Each of the two phases has a high melt entropy, and increases independently with a facet-like interface. Some eutectics from inter-metallic compounds and semi-conductors belong to this group.

In order to be able to directly observe the growth mechanism, Hunt and Jackson have undertaken analogy tests on transparent organic eutectics which indicate the same or similar ratio of the melting entropies of the two phases.

The eutectic of succinyl nitrile and borneol, analogous to the Al-Si system, solidifies with an irregular interface (photo 3.2). The facet phase (borneol) leads to the solidification. The second phase immediately follows the peaks, but is much later /16 at some points. The melting between the protrusions might only solidify with extensive undercooling so that there is a finer matrix at these points [33]. There is a striking similarity between photos 3.2 and 1.1.

### 3.32 Directed solidification

Conclusions on the solidification morphology of the Al-Si eutectic can best be drawn if the determining values for the crystallization, such as temperature  $G$  [ $^{\circ}\text{C}/\text{cm}$ ], growth speed  $R$  [ $\text{cm}/\text{sec}$ ] and composition of the melting, remain constant during the solidification test. This is best achieved with directed solidification [34,47-50].



Photo 3.2. Growth front of the succinyl nitrile-borneol eutectic [46].

Day and Hellawell [49] have carried out systematic analyses on highly refined Al-Si alloys with a wide range of temperature and growth rate variations. The analysis results are shown in photo 3.3.

Analyses of the growth front which were able to be made visible through sudden cooling, as well as X-ray and goniometric analyses of the silicon phase, led to dividing the diagram into three areas:

Area A: The ratio  $G/R > 10^7$  [ $^{\circ}\text{C sec cm}^{-2}$ ] forces a complete separation of the two phases. The silicon forms large facet-like crystals that are independent from each other which could grow in the directions  $\langle 100 \rangle$  or  $\langle 211 \rangle$ . The growth front of the Al is even and is only occasionally penetrated by previously crystallized Si. On the  $\{111\}$  surfaces of the Si, twin formation

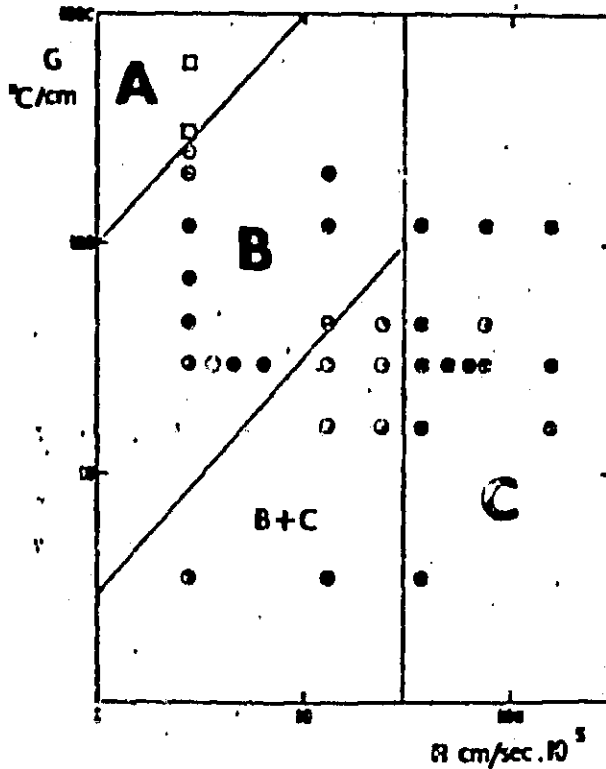


Photo 3.3. Classification of the growth of the eutectic Si according to the condition  $G/P$  [50]

has been observed. The diffusion paths between the individual Si-crystals are very long [50].

Area B: With values of  $G/R < 10^7$  [ $^{\circ}\text{C sec cm}^{-2}$ ], instabilities develop on the Al-interfaces which permits the Al-phase to grow cellularly, while the Si-phase forms rodlets which grow very parallel in the  $\langle 100 \rangle$  direction. The diffusion paths are small.

With a reduction of the temperature degrees and constant growth rate, matrix pictures develop in which the strong parallelism is loosened due to diagonally located Si-rodlets. These forms were also found by Bell and Winegard [47], as well as Cooksey, Day and Hellowell [48]. It was uniformly determined that the Si-phase leads to the solidification and that the Si-rods form a network.

Area C: For  $R > 3 \times 10^{-4}$  [cm/sec] the microsections show a matrix in which the Si occurs in completely irregular crystals or rodlets. The parameters that apply to area C correspond to those that are usually found in industry and laboratory castings. In this case, a stationary condition does not exist, that is, constant G and R. The view of Chadwick [41] that the Si phase is in the Al-matrix without any cohesion was able to be clearly refuted [49,51,52] especially through grid electron microscopic photos [49]. Precise examinations have shown traces of simple and repeated twin formation on the Si-crystals.

According to Day and Hellawell [49], a twin formation based on one crystal can appear on four different  $\{111\}$  surfaces, so that a total of five orientations are possible. The four newly developed orientations could then cause four further orientations through twin formations, of which only one agrees with the original orientation of the crystal.

/19

The number of possibilities makes the location of the silicon appear at random and without relationship, but the Si-rodlets are related to each other and relate to each other via twin-operations.

Day and Hellawell [49] interpret the existence of the twin in such a way that the silicon might have changed its growth direction during the solidification. In case the aluminum threatens to collect the silicon and overgrow, the silicon has the possibility to deviate so that it remains the leading phase and is not forced to reform a nucleus.

The possibility for changing the growth direction during the solidification is also reported for other systems (Ag-Si, Al-Ge [50] and Fe-C [53]).

### 3.33 Matrix formation with increased cooling rate

It has often been observed [34,51,54,55] that the morphology of rapidly cooled alloys and from refined alloys is very similar.

Day [34] was able to show that silicon has a "fern-shaped" form and was interrelated on deeply etched samples using the electron microscope.

### 3.34 Nucleus formation

In addition to systematic analyses by Crosley and Mondolfo [38] on the nucleus formation in pure Al-Si meltings, there is a series of publications [1,36,40,56] which deal with the question of the nucleus formation in technical Al-Si alloys. The authors assume aluminum phosphide crystals as foreign nuclei for the crystallization, since there is constantly a 15% excess phosphorus content on hand in technical alloys. The phosphite grid is similar to that of the silicon crystallographically and chemically, so that the prerequisites are fulfilled for the effectiveness as a foreign nucleus.

/20

Using electron microscope examinations and through X-ray micro-analyses, Imono [57] succeeded in proving that an active AlP-nucleus existed in nearly each silicon-primary crystal.

### 3.4 Enriching

In spite of the fact that the enriching of the aluminum-silicon alloys was already patented [58] in 1921 and since then has been used by industry in large amounts, the enrichment process has still not been unequivocally clarified.

The separation of the silicon in the form of small round crystals, the increase in the undercooling of 2-4°C in unenriched samples and up to 18°C below the eutectic temperature in enriched samples, as well as the apparent changing of the eutectic point



in the direction of higher Si-contents have been the reason for a number of studies.

Three theories essentially result from these studies which are used to explain the enrichment mechanism.

#### 3.41 Formation of the NaAlSi<sub>4</sub> phase

In the view of some authors [59-61], the enriched melt represents a ternary alloy in which the NaAlSi<sub>4</sub> phase is involved. Due to the presence of the ternary components, a finer distribution of the silicon results. Scheil [62], however, was able to compute the theoretical lowering of the freezing point which at 0.05°C was considerably lower than those observed from up to 18°C. Scheil was also able to show that the remelting of the alloy occurred at a higher temperature which does not indicate a ternary eutectic.

#### 3.42 Growth inhibition

This theory traces the enrichment effect to an inhibition of the growth of the eutectic silicon due to the sodium. 21

Edward and Archer [63] assume that the growth is mechanically inhibited due to the formation of a colloidal separation in front of the growth front or that the sodium is absorbed on the growth front and in this manner the growth process is more difficult for the eutectic silicon [64]. These statements are supported by the studies of Plumb and Lewis [65] as well as Tauscher [66], who discovered that the sodium is absorbed on the interface of the silicon.

Guyer and Phillips [67] explain the enrichment in that the silicon is already finely distributed in the silicon when separated and that the sodium prevents the agglomeration.

Thall and Chalmers [54] consider aluminum as the introductory phase in the crystallization. With the addition of sodium, the

interface energy between the aluminum and the silicon is reduced and thus the growth of the silicon is made easier.

Boom [68], on the other hand, recognized that in the solidification without the addition of sodium, the silicon is the leading phase. The addition of sodium, however, leads to a change in the control, whereby the silicon is finally surrounded by the aluminum. Due to the separation from the other melt, there is always the necessity for the silicon to form new nuclei. This theory is confirmed by the measurements of Davies and West [69,70] which confirm a lowering of the surface tension and a decrease in the wetting angle of enriched Al-Si alloys.

Another possibility of the growth inhibition is a lowering of the diffusion speed of the silicon through the addition of sodium. Tsumura [71] and Gosh, Wilcock and Kondic [72] trace the formation of the enriched matrix to this effect. Diffusion and viscosity measurements [73,74] in non-enriched and enriched melting show a diffusion inhibition with enriched melt even though the study results of the individual authors are very different.

/22

### 3.43 Inhibition of the nucleus formation of the silicon

This theory is based on the assumption that, due to the presence of sodium, the nucleus formation capability of the silicon is altered in that sodium contaminates the effective Si-nucleus.

It has been proven that the effect of P is weakened or neutralized [36] due to the addition of Na. After a specified "burn out time", in which the sodium evaporates from the melting, the nucleus-promoting effect of the phosphorus is again noticeable.

Kim and Heine [37] assume that the morphology of the silicon is dependent on the temperature at the growth front. The nucleus formation is impeded by the sodium, and the melting is undercooled

to the extent that the nucleus formation can start. The silicon then grows with a structure that is characteristic for the amount of undercooling.

Davies and West [69] not only see the cause of the enriched matrix in the inhibition of the nucleus formation, which results from the contamination of the nuclei that are important for the silicon, but assume a growth inhibition due to chemical absorption of the sodium on the silicon interface. The observed undercooling either leads to renewed silicon nucleus formation or to the further growth of the contaminated growth surface.

Also, Crosley and Mondolfo [38] combine nucleus formation inhibition and growth inhibition in their explanation of the enrichment mechanism. Also, in their view, the nuclei which are important for the silicon are contaminated. They consider it important, however, that the silicon is displaced as a leading phase which is viewed as a result of the diffusion inhibition. 23

As enlightening as some explanations for the enrichment may be in their details, they are, nevertheless, in contradiction to the studies of Bell and Winegard [75], Day [34] and Hellowell [49] which ascertained on deeply etched samples that, even with the addition of sodium, the eutectic silicon crystallized in filament shape and formed a cohesive branch. The authors observed the similarity of the structure with the rapidly cooled, non-enriched samples.

This information is not in agreement with the theories which are based on the alternation of the leading phase in the crystallization, and the resultant necessary new formation of nuclei for the silicon. A direct observation of the solidification with the heating table microscope should result in a determination.

#### 4. Tests

/24

##### 4.1 Test plan

In accordance with the objective of the study, the crystallization of aluminum-silicon melt is to be observed in the light microscope, and to the extent possible photographically registered.

For this, alloys of undereutectic (AlSi6), eutectic (AlSi 12.5) and overeutectic (AlSi 18) composition were selected in order to follow the growth of the primary crystallization phases and their effect on the eutectic reaction, in addition to the eutectic crystallization.

Also of interest were the change to the crystallization speed as a result of the varying of the cooling speed and the resultant changing matrix formation. They also intended to add phosphorus and sodium to the melt in order to make the crystallization visible.

Some melting tests on the alloys AgSi and AuSi should finally show to what extent the growth mechanism of the eutectic silicon is comparable in the alloys analyzed.

##### 4.2 Production of sample materials

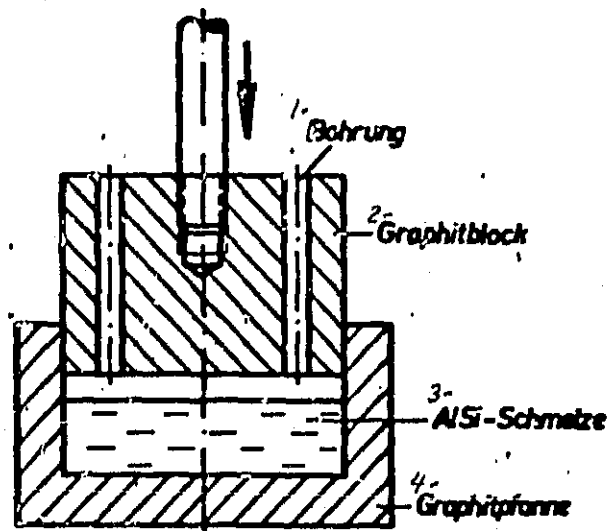
For the production of sample materials for the tests on the Al-Si alloys, aluminum with a purity of 99.998% and silicon with a purity of 99.99% were used, which is used in semi-conductors. The materials for use were weighed on an analysis scale and melted in a crucible of spectroscopically pure graphite in an induction furnace with a vacuum ( $10^{-4}$  Torr). After the melting, a graphite block with 20 borings with a diameter that correspond to the inner diameter of the crucible used in the heating table was lowered with a slicker and brought into contact with the ladle.

/25

ORIGINAL PAGE IS  
OF POOR QUALITY

After a short time, the graphite block was heated in the induction field. It was then slowly pushed into the ladle, whereby the melting filled the bored holes (photo 4.1). After the cooling, the individual rods were able to be removed from the block. Then they were sawed off, polished on all sides, and examined for their matrix in the microscope.

Photo 4.1:  
Lowering of the  
graphite block.



1--boring 2--graphite block 3--Al-Si melt 4--graphite ladle

The alloying of the other materials examined, whose purity was stated at a minimum of 99.99%, was carried out during the testing on the heating table.

#### 4.3 Test description

The first heating table microscopic tests encountered unexpected experimental difficulties. The first method, which measured the testing temperature by means of a thermoelement using design factors of an available heating table which is guided from below to the crucible, proved to be unusable, since the deviations between the actual and the indicated temperature amounted to several 100°C. It was also initially very difficult to identify the particles forming during the solidification, since individual crystals floating freely on the melting surface do not have to agree in appearance with those known from micrographs from large samples and must agree with hypothetical forms

/26

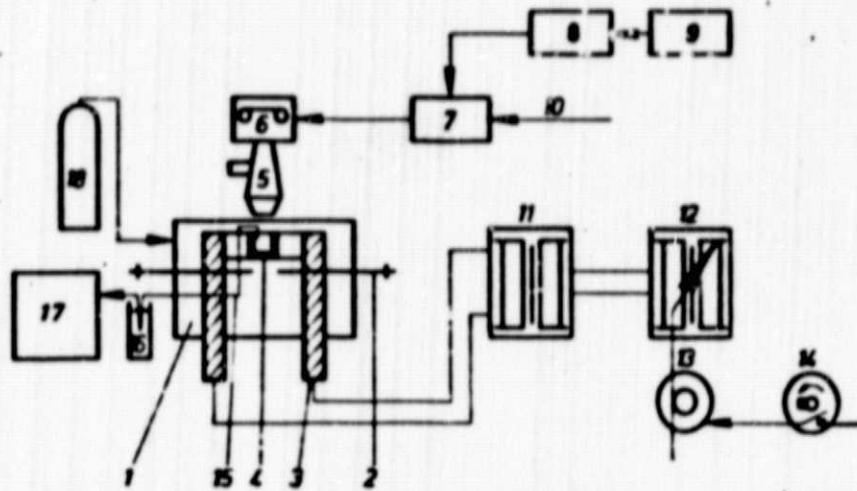
due to mutual influence during the solidification. Thus, after lengthy tests it was found that the presumed eutectic reaction that was observed at first was only the crystallization of the oxide film floating on the melting (and could hardly be distinguished from it) and thus the actual reaction was concealed. Using a high vacuum, they successfully removed part of the oxide skin and were able to observe the eutectic solidification of the alloy melting. The question was how to eliminate this oxide film or to be able to avoid it from the start. All attempts to bring the samples into the testing areas as clean as possible without coming into contact with oxygen were unsuccessful, since the aluminum was already covered with an oxide layer after a few seconds, and the placing into the heating table could only occur in the air.

The melting area of the heating table appeared to be too small for any mechanical elimination using manipulators. Thus, failure led to a search for other eutectic systems with which the inclination toward oxygen was lower. Of the alloy systems in question, the system silver-copper presented itself. Here they were successful in photographing the course of the solidification. Since, however, the silver-copper system has a eutectic with very fine lamella formation, the lamellae were not easy to recognize, which resulted from the small aperture of the lens which had a negative effect on the capability for analysis. This small aperture, however, is determined by the required work distance between the melting surface and the lens which with normal lens can only be realized through the enlargement of the focal distance.

During the examinations on the silver-copper system, discussions were held on the elimination of the oxide skin of the Al-Si melting using manipulators. With the available heating table, they were successful after considerable effort to at least partially remove the oxide skin using complicated manipulators and thus to leave the melting surface partially visible. Inspired by this, they started the construction of a new enlarged heating

/27

ORIGINAL PAGE IS  
OF POOR QUALITY



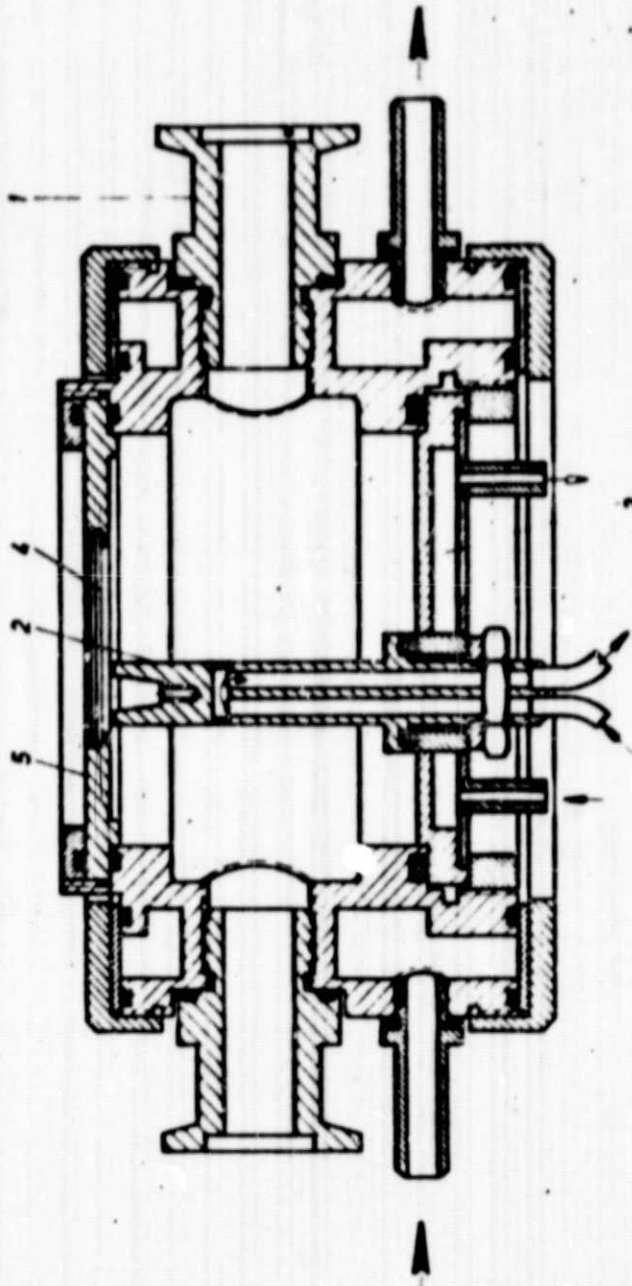
- |               |                     |                                 |
|---------------|---------------------|---------------------------------|
| 1 Heiztisch   | 7 Automatik         | 13 Potentiometer mit Stellmotor |
| 2 Manipulator | 8 Frequenzumsetzer  | 14 Motor mit Schaltknochen      |
| 3 Elektrode   | 9 Frequenzgenerator | 15 Mantelthermoelement          |
| 4 Tiegel      | 10 Fußschalter      | 16 Vergleichsstelle             |
| 5 Mikroskop   | 11 Festtrafo        | 17 Kompensationsschreiber       |
| 6 Kamera      | 12 Regeltrafo       | 18 Argon                        |

Photo 4.2: Schematic drawing of the test facility

- |                 |                        |                                  |
|-----------------|------------------------|----------------------------------|
| 1 heating table | 7 automatic            | 13 potentiometer with servomotor |
| 2 manipulator   | 8 step-down frequency  | 14 motor with trip cam           |
| 3 electrode     | 9 frequency generator  | 15 sheath thermometer            |
| 4 crucible      | 10 foot switch         | 16 reference point               |
| 5 microscope    | 11 fixed transformer   | 17 compensation printer          |
| 6 camera        | 12 regular transformer | 18 argon                         |

table system. The system offered more space and made mechanical and chemical melting treatment possible through manipulators operated from the outside as well as a direct measurement of the temperature using a sheathed thermometer submerged in the melt.

The heating table is on a cross table that can be moved with /29 a micrometer screw. It is designed with two walls for the purpose of water cooling. There are five flanges in the wall which serve for the housing of the manipulators that are operated from the outside, the input and exhaust of buffer gas as well as the operation of the sheathed thermal element. The copper electrodes are also water-cooled and are diagonally isolated and placed



- 1 flange
- 2 electrode
- 3 floor plate
- 4 quartz glass printer
- 5 swivel lid

Photo 4.3: Heating table



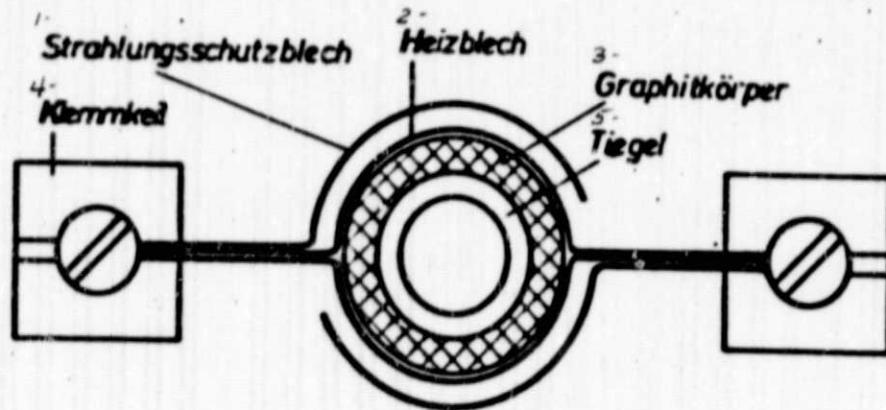
eccentrically on a special floor plate. The resistance-heated heat steel made of tantalum (thickness: 0.05 mm) is fastened to the electrodes with the help of clamping wedges. These heat-sheets surround the crucible. There is a quartz glass plate in the cover above the crucible so that the special lens corrected for this plate is placed directly above the sample without being damaged or destroyed by the radiated heat. The entire cover can be turned during the melting process. Due to the eccentric position of the sample, a clean sector of the disc can always be placed in the ray of the microscope in case metal vapors from the sample condense or sublimate on the quartz disc.

/29

The vertical microscope with a xenon-high pressure lamp as a light source is located above the heating table. The light-stream experiences a dispersion in the binocular tubes of the microscope. The photo supports of the tube contain 80% of the total light and the ocular supports 20%. A fully automatic camera for micro-photography rests on the photo supports. The automatic device controls the exact regulation of the illumination over a photo reproducer when the lever is activated as well as the vibration-free opening and closing of the electromagnetic camera shutter and the film transport by one photo length after the closing of the shutter. The camera can be released with the help of a frequency generator and a frequency reducer through time-constant impulses or by simple foot switches.

The heating current for the tantalum sheet is provided by a fixed transformer which is connected to a regulating transformer. This can be controlled by hand or by a thyristor from outside. It had first been attempted to regulate the linear cooling with the help of a time planning device. As a result of the low thermal inertia of the sample, which was due to the low sample weight and as a result of the fact that the values of the control section with regard to the changing degree of oxidation of the tantalum-heating sheet during the test had not been kept constant, the results were not satisfactory. Therefore a control mechanism

/30



1--radiation 2--heating sheet 3--graphite substance  
4--clamping wedge 5--crucible

Photo 4.4: Position of the crucible in the heating table

was used which was based on the principle that the ignition time of the thyristor was altered with the help of a potentiometer which was connected to a servomotor. The servomotor received signals via a switch cam which was located on a slowly turning electromotor. It was possible to vary the cooling speed by the number of the activated switches per revolution.

The controlling of the test temperature and the cooling rate was accomplished on a line-compensation printer via a sheath and thermoelement which has dipped directly into the melt. With the release of the camera an impulse was simultaneously given to the printer so that it was henceforth possible to relate the photos to the appropriate temperature.

For better thermal insulation, the test crucible of  $Al_2O_3$  was placed in a substance of spectrally pure graphite. The heating sheet surrounded the graphite substance (photo 4.4). With higher melting alloys, i.e., AgCu and AgSi, radiation protective sheets have proven themselves; this was not necessary with the alloy AlSi.

In order to eliminate the oxide skins which prevent the observation of the crystallization, a wire loop made of tungsten was used that was fastened to one of the manipulating devices.

Although a complete elimination was not possible, it was, nevertheless, possible to remove so much of the oxide skin so that the surface of the sample was only covered with a thin transparent layer. /31

The tests were not carried out in a vacuum, as is often the case for heating table microscopic examinations, but in an argon atmosphere of 500 Torr in order to be able to extensively exclude the influencing of the results by the changing of the chemical composition of the sample as a result of selective vaporization. The special-argon with an oxygen content of <3 vpm obtainable in steel bottles proved to be the best. The feed from the steel bottle into the test area was via gas-tight copper tubes. After the insertion of the sample substance, the test area was evacuated with the help of a water jet pump and kept under flowing argon for about 30 minutes. During the test the argon inlet valve and the outlet valve were closed.

The planned chemical melt treatments were carried out at a temperature of 700°C using the manipulators. Red phosphorus was filled into a ceramic tube which was dipped into the melt. In the addition of sodium to the melt, there were difficulties due to the high vaporization pressure of sodium since the vapor condensed on the quartz plate and made viewing impossible. Therefore, a salt mixture of NaF, NaCl and KCl was used which forms a melt ternary eutectic at  $T = 605^{\circ}\text{C}$ . This salt mixture was added by using the manipulating devices. After the solidification, it was determined that the sample had been adequately enriched through metallographic microsection examinations. /33

## 5. Test results<sup>+</sup>

### 5.1 Al-Si 18

---

<sup>+</sup>The heat table microscopic photos are compiled in a special photo section in Chapter 8.

Photos 8.01 and 8.02 show the growth front of a eutectic silver-copper alloy which is crystallized at a rate of  $R=8 \mu\text{m}/\text{sec}$  at  $T = 779^\circ\text{C}$ . The parallel lamellae can be clearly seen but the details on whether one of the two phases lead to the solidification is not clear due to the limited resolution capacity of the special lens.

The lamella structure of the alloy is also recognizable in the micrograph (photo 8.03) so that the action here on the surface can be viewed as being representative for the interior of the sample. The definition of the individual eutectic crystals in the sense of the Scheil definition of a normal eutectic is also clearly identifiable in the micrograph.

## 5.2 Al-Si Alloy

### 5.21 Al-Si 18

Photos 8.11 to 8.16 show the growth of a silicon primary crystal at a cooling rate of  $T = 5^\circ\text{C}/\text{min}$ . The predominant polygonal crystal shape leads to the conclusion that the melt has a slightly higher temperature than the crystal, and the released crystal heat is abducted in this manner. With a crystal front that is not even, a growing crystal area would reach an area of higher temperature which would lead to a reduction in the growth rate.

The growth was in three dimensions, as was determined with metallographic microsections parallel and vertical to the surface as well as through stratified layers from the surface.

Due to the low specific weight compared to the melt, the primary crystals float on the surface and with increasing volume protrude out more and more (iceberg effect) which is clearly shown in these photographs.

/34

The starting points for the silicon primary crystals were not recognizable in the heating table microscope, but it can be said that the crystallization on the rest of the oxide skin was obviously easier than on a "cleaner" part of the surface.

With an increase in the cooling rate, the number of silicon primary crystals increased while their size decreased.

#### 5.22 Adding of phosphorus to the AlSi 18-melting

An addition of phosphorus to the melt already leads to the formation of a large number of silicon-primary crystals at low cooling speeds. This "refining process" is depicted in photos 8.21 to 8.28. The phosphorus itself and the AlP phase are not recognizable, but the clear multiplication of the silicon primary crystals lead to the conclusion that phosphorus is favorable for seed formation on primary silicon. Phosphorus thus works similarly to an increase in the cooling rate on the primary silicon while an effect on the eutectic silicon was not able to be detected.

With regard to the eutectic silicon, it is visible from photos 8.21 to 8.28 that its growth is due to the primary silicon.

#### 5.23 AlSi 12.5

Photos 8.31 to 8.35 depict the crystallization process in a eutectic aluminum-silicon alloy at a cooling rate of  $T = 5^{\circ}\text{C}/\text{min}$  and photos 8.41 to 8.47 at a cooling rate of  $T = 94^{\circ}\text{C}/\text{min}$ .

The eutectic silicon phase initiates the solidification and grows dendritically. The growth is not at all continual but rather jerky. A dendritic branch begins, remains for a short time and then begins to branch off along its entire length at angles of about  $60^{\circ}$ . The side branches grow into the melt, remain and branch off. In this manner, a silicon-network develops starting

from the growth center. This process is clearly recognizable at low crystallization rates.

The dendritic growth requires an undercooling of the melt below the equilibrium temperature. This was registered during the tests and amounted to 2 to 4°C with a cooling rate of 15°C/min. Low undercoolings (2-3°C) were observed with the AlSi 18 alloy and somewhat higher values (3-4°C with AlSi 12.5. This is due to the absorption. With the alloy AlSi 18, the eutectic reaction begins entirely on the silicon primary crystals (photos 8.24 to 8.26). Obviously, there are good possibilities for the growth of eutectic silicon so that cooling required remains low. With the alloy AlSi 12.5 the possibility of the growth does not exist but the formation of seeds capable of growth does not appear to offer any difficulties as the cooling which only increase very little indicates.

At higher cooling rates (100°C/min), the values for the undercooling easily increase by 2-3°C.

From photos 8.31 to 8.35 and 8.41 to 8.47, it can be seen that few seeds are already adequate in order to initiate the crystallization of a large portion of the alloy.

In viewing photos 8.31 to 8.35 and 8.41 to 8.47, it can be seen that the volume ratio of aluminum:silicon = 7:1 is not maintained. This is certainly an effect of the open upper surface.

In the transition from the liquid to the solid phase silicon experiences a volume increase. The lower pressure on the surface results in less resistance to the crystallization of the eutectic Si-phase so that it can "expand". In addition to that the specific lighter silicon compared to the melting collects on the surface due to the gravity refining and protrudes slightly out of it. The Al-phase experiences a volume contraction in the solidification which leads to the aluminum seeping into the Si-network.

/36

Photo 8.36 shows the matrix from photos 8.31 to 8.35 after slight sputtering of the material. In the middle a maximum of 1  $\mu\text{m}$  was removed and more on the left and right edge, since it was originally a slightly concave surface. The classification of photo 8.35 and photo 8.36 is easily possible. On the left edge of photo 8.36 a transition into deeper regions takes place until there is a matrix as is known from metallographic micrographic photos of eutectic AlSi-alloys. In the transition, however, it can be seen that the dendritic growth also continues in the depth. In photo 8.37, this transition at other points is even shown in greater enlargement.

A comparison of photos 8.31 to 8.38 and 8.41 to 8.48 indicates that with increasing cooling and crystallization speed the Si-branch becomes continually more refined. Simultaneously impressions of Al-primary dendritic crystals develop similar to the observations by Gurtler [36] which are surrounded by the eutectic silicon (photos 8.41 and 8.45).

#### 5.24 AlSi 6

As already mentioned, it was extremely difficult to observe the solidification of undereutectic alloys since the oxide accumulation was very heavy due to the high Al-content.

It was also not possible to recognize floating Al-primary crystals floating freely in the melting since the melting and the crystal do not have different colors. Not until later in the process of solidification, especially at the start of the eutectic reaction, do the shapes of the Al-dendrites emerge from the melting (photos 8.51 and 8.52). Photo 8.53 shows the solidified alloy at room temperature and photo 8.54 the removed surface of about 2  $\mu\text{m}$ . The eutectic silicon grows into the crevices of the Al-dendrites. This, as well as the surrounding of the impressions by Al-dendrites (photos 8.41 to 8.45) leads to the presumption that the seed formation of the eutectic silicon is not assisted by Al-primary crystals.

## 5.25 Crystallization rate

The rate of crystallization  $R$  of the eutectic silicon, which was determined as a function of the cooling rate  $T$ , and is intended as a measurement of it, determined how quickly they remove the heat from the system. The cooling rate was able to be determined from the temperature printer. The crystallization rate was determined from the path which was taken by the growth front between two photos and the time between them. Since the camera was controlled by a constant time impulse with the help of a frequency generator, this value was presupposed. The path was determined from the weight of the surface which had coated the growth front between the two photographs. The result is shown in photo 5.1.

In spite of the wide dispersion, it can be seen that the rate of crystallization is proportional to the root of the cooling rate.

Through a precise analysis the cause of the dispersion was able to be determined. In photo 8.45, a dendrite can be seen which grows from the continuous growth front and even with an increased growth rate.

The values for the rate of crystallization are too high for the diagram. If the accelerated dendrites are not considered then values are obtained which are on the line. Deviations downward develop if two fronts grow successively. The rate of growth slows before they meet. This effect is noticeable at a distance of 10-20  $\mu\text{m}$ .

## 5.26 The interdendritic interval

The relationship established by Day [34] and Hellawell [50] between the rate of crystallization  $R$  and the interdendritic interval

$$\lambda = 0.14 \cdot R^{-0.56}$$



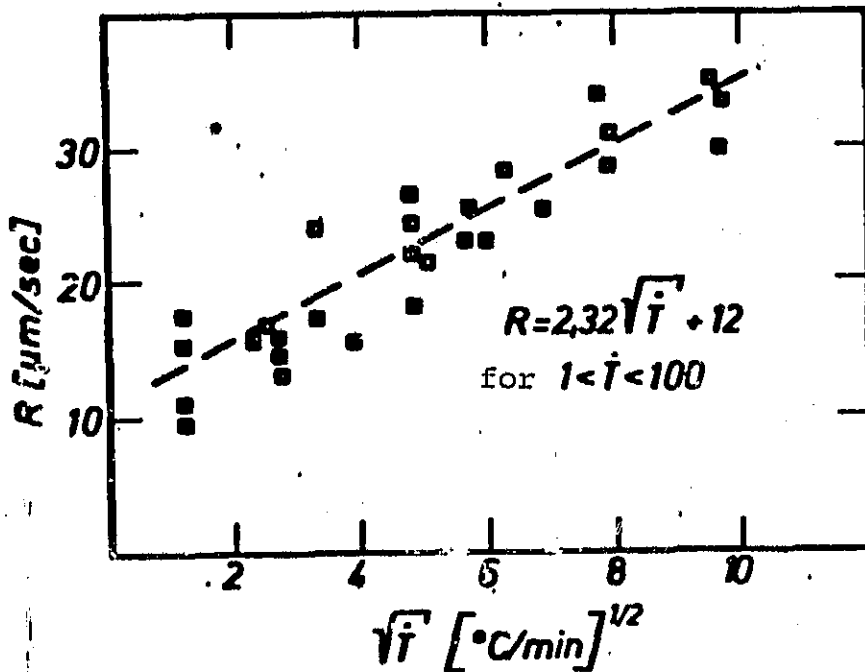


Photo 5.1: Relationship of the rate of crystallization of the eutectic silicon to the rate of cooling

was able to be confirmed by the measurements. The measurement values are partially on the line and partially in the extension to the Day and Hellawell line (photo 5.2). The lower line shown in this diagram applies to the lamella interval with normal eutectics. With the same rate of growth  $R$ , the lamella interval of normal eutectics is smaller than the interdendritic interval of abnormal eutectics which can be explained by the close coupling of the crystallization phases in lamella solidification.

#### 5.27 Adding of sodium to the AlSi 12.5 melting

The observation of the crystallization of the alloy AlSi 12.5 with the addition of sodium was very difficult. The undesirable effects of the high steam pressure of metallic sodium were able to be avoided through the use of a mixture of NaF, NaCl and KCl as an enriching salt, but the salt mixture crystallized at a ternary eutectic temperature of  $T = 605^{\circ}\text{C}$  and thus earlier than the

ORIGINAL PAGE IS  
OF POOR QUALITY

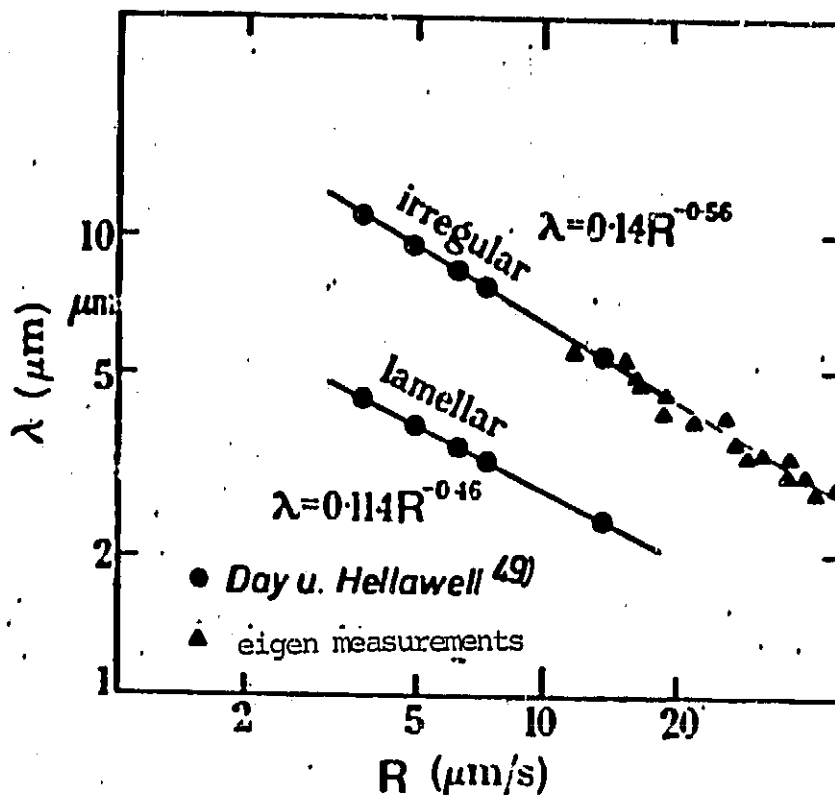


Photo 5.2: Relationship of the interdendritic interval of the silicon to the rate of crystallization

AlSi 12.5 alloy. Nevertheless, they succeeded in observing and photographing the solidification running below the firm, partially transparent salt crust a few times (photos 8.61 to 8.63). The most striking result is that the crystallization mechanism is obviously the same as for non-enriched alloys despite the presence of sodium. The eutectic silicon continues to grow dendritically and leads to the solidification. It is noteworthy, however, that the crystallization rate of the enriched AlSi 12.5 alloy at  $R = 65 \mu\text{m/sec}$  with a cooling rate of about  $20^\circ\text{C/min}$  is exceptionally high which might be due to the undercooling. This could not be measured using the thermoelement since the melt containing Na was very aggressive and destroyed this. With regard to the heating output, however, it was able to be determined that greater undercoolings developed than in non-enriched samples. In addition to the large undercooling and the high rate of crystallization,

the very fine branching of the silicon is striking which only developed with the non-enriched samples with high cooling rates.

One thing should be especially pointed out which was observed at increased cooling rates and in the enrichment with Na-salt.

A comparison of the photos 8.46 with 8.47 and 8.62 with 8.63 shows that the Si-phase that originally grew in a network and dendritically no longer appears to be continuous at room temperatures (photo 8.47 and 8.63).

Shortly after the solidification of the silicon there is a separation of the side branches from the main branches of the dendrites and then a coagulation. This process takes place during a period which was considerably longer than the crystallization time. It often lasted a few minutes until the Si-particles had assumed a conical shape. As a result of the fineness of the Si-branch and the limited resolution of the microscope, the process was very difficult to recognize. /41

It should also be mentioned that some enrichment processes with bismuth as the enrichment element brought no change in the growth characteristic of the eutectic silicon. The microsections showed the typical enriched structure whereby individual Al-primary crystals could be seen in dendritic shape in addition to the very finely dispersed Si-phase.

#### 5.28 Raster scan electron microscopic photographs

The photographs which were obtained from anodically removed samples using an electrolyte of 80 ml ethanol and 20 ml of perchloric acid at  $T = -10^{\circ}\text{C}$ , are shown in photos 8.71 and 8.76. In this case, the Si-phase appears bright.

Photo 8.71 shows a sample that was cooled at  $50^{\circ}\text{C}/\text{min}$ . The Si-phase forms a relatively rough structure composed of sheets

and rods. With an increase in the cooling rate to 94°C/min, the eutectic silicon is considerably finer. However, it is also clear here that the Si-phase solidifies continuously (photo 8.72). Photo 8.73 shows a sample cooled at about 20°C/min which was enriched with sodium. Here it is worth noting that the Si-phase forms a thread-shaped network that is linked together.

The similarity of the rapidly cooled non-enriched and the enriched samples should be made clear by photos 8.74 to 8.76.

Photo 8.74 shows the same Na-enriched sample as photo 8.73 but with a 10-fold enlargement. A similar formation of the Si-phase is obtained with high cooling rates (photo 8.75). Here a droplet of an AlSi 12-5 alloy from the liquid state was cooled in water of 700°C. Photo 8.76 shows that even with extremely high cooling rates, as those that can be achieved in a shockwave device with  $10^5$  to  $10^6$  °C, the Si-phase solidifies in continuous form and crystalline.

#### 5.4 AuSi 4 alloy

The crystallization of the eutectic silicon in the AuSi4 alloy is shown by photos 8.91 and 8.92. The structure of the Si-phase is very fine and is at the limit of the resolution capability of the microscope. There is a certain similarity to the enriched Al-Si alloys which is also recognizable from the longitudinal section (photo 8.94). The simultaneous development of primary gold and silicon crystals is a peculiarity. This is a result of the gravity refining.

The seed promoting effect of the primary gold on the eutectic silicon is noteworthy.

/43

#### 6. Discussion of the test results

/44

On non-enriched Al-Si alloys, Korber [2] has found an extremely poor wetting situation between the crystallized silicon and the eutectic melting at a wetting angle of  $130^\circ$  as well as a relatively high diffusion coefficient for the silicon, and the latter indicates a high mobility of the silicon in the melting. It is, therefore, not surprising that the silicon is clearly the leading phase in the eutectic crystallization. There do not appear to be exceptional difficulties in the seed formation as can be concluded from the slight undercooling below the eutectic temperature at low cooling rates. Since one single seed is also sufficient to initiate the crystallization of a large portion of the volume, the number of seeds that are necessary need not be too high. Due to the dendritic growth the eutectic silicon in the aluminum matrix forms a branch extending from the present growth center which is partially continuous [34,47,52].

The ratios in the enrichment were different. With the addition of sodium, Korber [2] observes a reduction in the surface tension by about 25% and a decrease in the wetting ratio to  $44^\circ$ , thus to about 1/3 of the original value which indicates a very good wetting situation between silicon and melting and which clarified the very fine branching of the silicon. The silicon movement is considerably limited which is shown by the reduction of the diffusion coefficient by 40%. These factors actually help the penetration of the Si as the phase initiating the solidification by the aluminum. The examinations in the heating table, however, show that this does not result. The silicon also grows dendritically in the presence of Na. Wamich and Winterhager [56] were able to make the superior seed-forming capacity of the Si in the comparison to aluminum clear.

/45

The increased growth rate of the aluminum seldom becomes important due to the formation of Al-dendrites since the Al-growth is inhibited by the Si-wetting. In addition to the difficulty for the aluminum to form seeds capable of growth, the early Si-

crystallization leads to a back-up of contaminants which further lowers the solidification temperature of the Al.

According to Korber, Na is active at the interface which leads to an enrichment of Na at the Si/melting interface. The reduced diffusion rate indicates that the insertion of silicon atoms at this interface that is enriched with Na is made more difficult or even impossible.

The silicon is not successful in penetrating the "armor" of Na until there is an undercooling. If this has occurred, then the silicon grows dendritically whereby the reduced interface tension leads to the formation of a very fine Si-branch. A confirmation of this view is rendered by the examinations in which it was able to be clearly shown that even in alloys that are enriched with Na the silicon forms thread-shaped crystals which are connected to each other [34,48,75].

The crystallization of non-enriched Al-Si alloys at a higher cooling rate and of enriched Al-Si alloys is, therefore, thoroughly comparable. The only difference is that the greater undercooling due to a higher cooling rate leads to a growth which takes place below the equilibrium temperature and in which the diffusion rate of the silicon has been reduced through the temperature effect alone. The growing dendrite tries to equalize the unequal state in that it shortens the diffusion paths due to strong branching and its surface enlarges in order to make the increasing insertion of Si-atoms possible.

Na reduces the diffusion speed of the silicon also without undercooling and prevents its insertion through a build-up of Na in front of the growth front. The reason for the fine branching of the growing silicon is not only to be sought after in the inequality as a result of the undercooling, but the sodium itself causes these. The reduction of the moistening angle, which is clearly expressed through a better contact of the silicon with

/46

the melting, means an increase in the surface of the silicon, and thus a finer branching which is only intensified by the under-cooling.

The addition of sodium has two contrasting effects as a result: the diffusion speed of the silicon is reduced, and the sodium itself serves to improve growth capabilities through improvement of the exchange surfaces.

As Wamich and Winterhager [56] have shown, the content of the sodium in the melting may not exceed a specific amount. In this case, the built-up sodium could become so thick in front of the growth front that growth finally stifles itself due to the lack of a supply of atoms. While the sodium cloud is being built up, pure aluminum solidifies in the "over enriched" bands.

The diffusion inhibiting effect of the sodium as a cause of the enriched matrix is also indicated by the tests in which an enriched matrix could no longer be achieved in spite of the addition of sufficient sodium at very slow cooling rates [38,71] because in spite of the decreased diffusion due to the sodium cloud due to the longer time available, enough silicon atoms were able to be diffused at the interface.

The assumption by Wamich and Winterhager [56] that with decreasing cooling rates, the increasing influence of the reduced interface tension leads to a reduction in the Si-seed formation and thus to an increase number of seeds, was not able to be confirmed in our own studies. /47

Day [76] was able to show with an AlSiCu-alloy that the number of cells per area, which can be viewed as a measurement for the number of effective seeds, did not change in the alloy endowed with sodium compared to the non-enriched alloy, whereby the cooling rates in both cases were the same.

On the other hand, Engler [77] was able to confirm a decreasing number of seeds in enriched samples compared to non-enriched through quenching tests. From this he concludes that the physical states of the eutectic matrix result from the interaction of seed formation and crystal growth "without character differences existing between them".

This appears in fact to be a clear explanation. A possible "contamination" of heterogeneous seeds due to sodium acting at the interface has the same effect as an impediment to the combining of several atoms at the same time in the same place on a critical seed nucleus due to the reduced movement of the silicon caused by sodium.

It is difficult to interpret the melting and coagulation processes which were observed on non-enriched alloys at high cooling rates and on enriched alloys. There is possibly an explanation here for the isolated appearance of the silicon in the microsection.

This appearance on organic substances was first observed by Papetrou [78]. After further studies, partially on organic [79] and partially on metallic [80,81] substances, the following were presumed to be reasons for the remelting of the branches on the dendritic system:

1. Insignificant concentration movements in the branching area leads to a slight reduction in the melting temperature and to altered solubility conditions in the surrounding melting.
2. The effort of a system to effect the state of the lowest energy leads to the constriction and coagulation due to the effect of the surface tension.

48

The crystallization heat that is released will support the constriction and coagulation process. In the case of the silicon, it is unusually high.



Due to the extraordinary fineness of the silicon branch, it is probable that even the small curvature radii on the branch positions lead to solubility conditions which support the processes.

A careful assessment of the melting rate permits the acceptance of values by Korber [2] which he had obtained through the dissolving of Si-discs in an AlSi 9 melting at a temperature of 680°C. Only fractions of seconds were necessary at this temperature for the melting of dendritic branches. At lower temperatures and in an AlSi 12.5 melting the time was lengthened corresponding to the dependence of the temperature of the diffusion coefficients and the altered saturation concentration.

In spite of the different possibilities, it is probable that the melting and coagulating of the dendritic branches is a process which is brought about by the free surface or at least requires it. This is indicated by the continuous Si-branch as was able to be clearly shown in the raster scan electron microscope photographs. The fact that places were usually found on the surface sputterings where the Si-particles were in contact with each other also indicates that the manifestation is a surface effect.

With information on the growth characteristics of the Si, 49  
the technical designation of "lamellar silumin" is not justified in the sense of the Scheil definition, at least if the lamellar crystallization of the alloy AgCu is observed. "Lamellar silumin" is thus only a photographic difference to the "granular silumin".

The studies of this with an alloy enriched with phosphorus could confirm that phosphorus has a seed-forming effect on silicon and thus provides a further contribution to the support of the phosphide seed theory. According to the studies by Imono [57], there could hardly be any more doubt about this theory.

The reports by Chiu [82] and Pillai [83] that other materials also cause an enriching effect were able to be confirmed through

tests with bismuth as an enrichment element. The reason for the enrichment might be found in this case just as with sodium in the growth inhibition of the silicon.

If after the examinations in this study all the questions about Al-Si alloys cannot be answered, nevertheless, the problem of the sodium enrichment appears to be solved in principle. The heating table microscope has contributed to this to a significant degree. It is conceivable that even with other problems that are still pending, such as the effect of sulfur on the iron-graphite-eutectic, additional information has been made possible with this method of examination.

## 7. Summary

The crystallization process of aluminum-silicon alloys was examined in this study in the high temperature microscope. These examinations were supplemented by the observation of the crystallization of eutectic AgCu, AgSi and AuSi-alloys. 50

Silicon-primary crystals grow in overeutectic AlSi melting in polyhedral form. The addition of phosphorus to the melting confirms the strong seed-effect of this element on silicon.

The Si-phase grows dendritically in the eutectic reaction and leads to the solidification. Primary silicon clearly has a seed forming effect on the eutectic Si-phase but not on primary aluminum.

At high cooling rates, a fine branching of the eutectic Si-dendrites develops as a result of the strong undercooling.

The eutectic Si-phase also grows dendritically in alloys "enriched" with sodium. The fine branching is traced to the undercooling resulting from the reduced diffusion speed of the silicon as well as to the improved wettability between silicon and the melting.

The examinations carried out using the grid scan electron microscope confirm that the Si-phase also solidified as a continuous network in the interior of the sample whether a sample is enriched or not.

Melting and coagulation processes were observed on the branches of the dendrites. It is assumed that this is an effect of the free surface.

In the crystallization of the eutectic silicon of the alloys Ag-Si and Au-Si, similarities as well as differences to the alloy Al-Si were observed.

/51

In cooperation with the Institute for Scientific Film in Gottingen, a 16mm film was made which shows the crystallization of the Al-Si alloys.

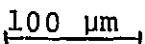
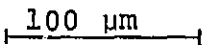
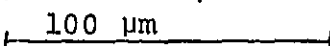
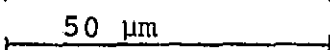
## 8. Photo part

/52

### Preface

The heating table microscopic photographs are presented on the following pages. The Si-phase appears dark on a light background.

The heating table photographs have an original size of  $V = 320 : 1$ . With the microsection photographs, other enlargements were necessary in some cases. The scales indicated correspond to the lengths:

V = 200	
V = 320	
V = 500	
V = 1000	

ORIGINAL PAGE IS  
OF POOR QUALITY

In the grid scan electron microscopic photographs, the Si-phase appears light on a dark background. The scales indicated correspond to the lengths:

V = 900      20  $\mu\text{m}$

V = 9000     2  $\mu\text{m}$

8.0 Eutectic crystallization of the AgCu alloy

/53

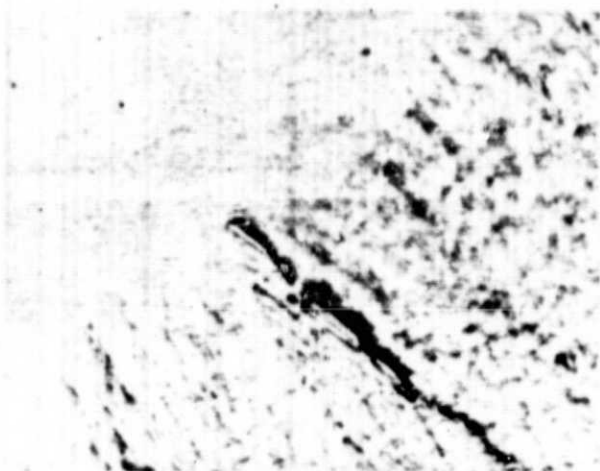


Photo 8.01:

T = 779°C

V = 320

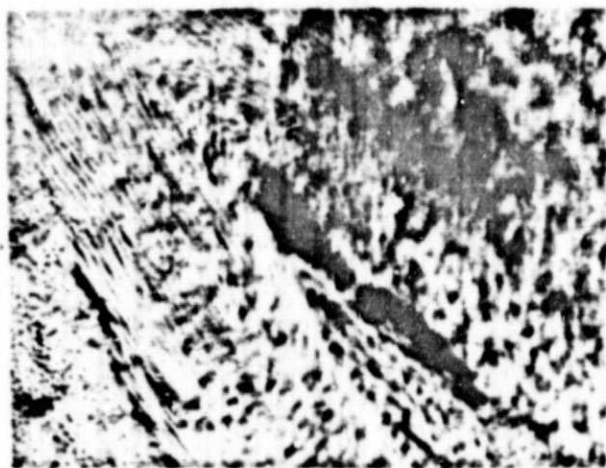


Photo 8.02:

T = 779°C

V = 320

ORIGINAL PAGE IS  
OF POOR QUALITY

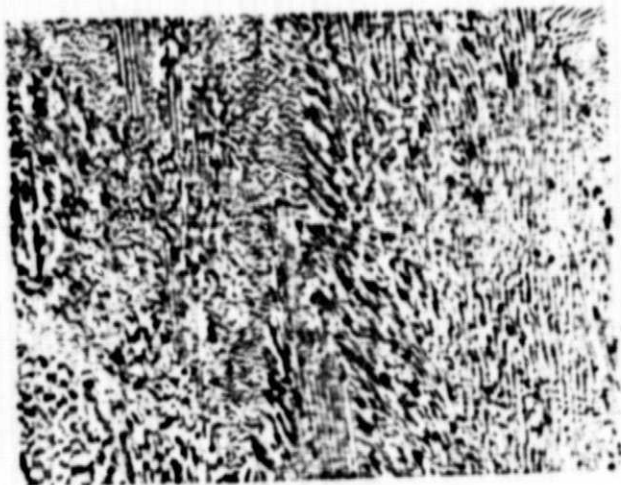


Photo 8.03:  
Longitudinal microsection  
Cu-phase:  
dark  
V = 320

### 8.1 Crystallization of the AlSi 18 alloy

Growth of the Si-primary crystals, cooling 5°C/min.



Photo 8.11:  
T = 660°C  
V = 320



Photo 8.12:  
T = 640°C  
V = 320

ORIGINAL PAGE IS  
OF POOR QUALITY



Figure 8.13:

T = 620°C

V = 320

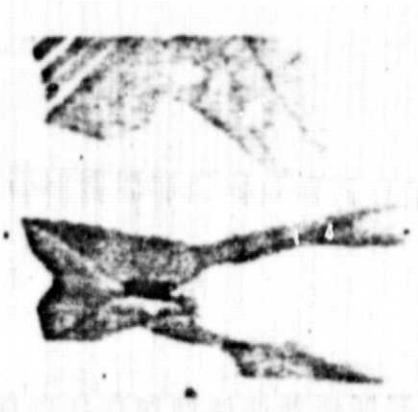


Figure 8.14:

T = 500°C

V = 320



Figure 8.15:

T = 577°C

eutectic reaction

V = 320

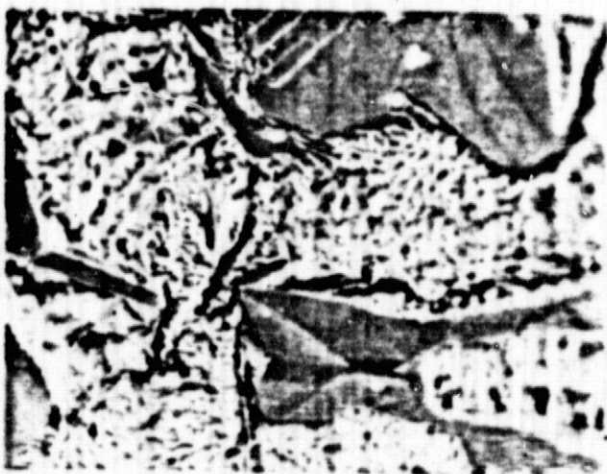


Figure 8.16

Room

Temperature

V = 320

ORIGINAL PAGE IS  
OF POOR QUALITY

8.2 Crystallization of the AlSi 18 alloy

/56

Addition of phosphorus, cooling 5°C/min



Photo 8.22: T = 620°C V = 320



Photo 8.24: T = 577°C V = 320



Photo 8.21: T = 660°C V = 320



Photo 8.23: T = 577°C V = 320  
start of the eutectic reaction



ORIGINAL PAGE IS  
OF POOR QUALITY

57



Photo 8.25: T = 577°C V = 320



Photo 8.26: T = 577°C V = 320



Photo 8.27: room temperature (V) = 320



Photo 8.28: longitudinal microsection  
V = 200



ORIGINAL PAGE IS  
OF POOR QUALITY

8.3 Eutectic crystallization of the alloy AlSi 12.5,  
cooling 5°C/min

/58



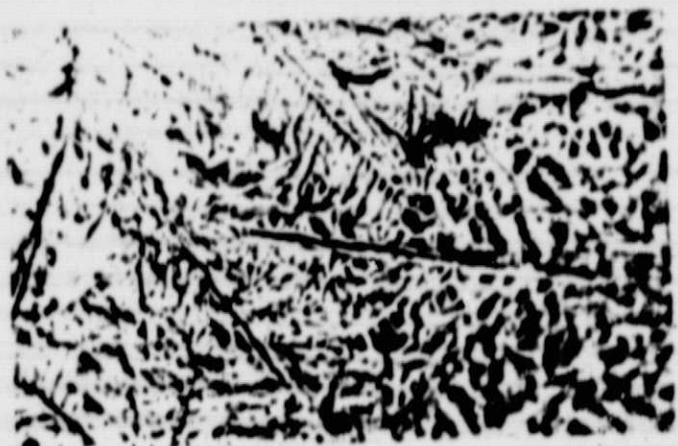


Photo 8.35: room temperature  $v = 320$



Photo 8.36: Surface cutting  $v = 320$



Photo 8.37: surface cutting  $v = 500$



Photo 8.38: longitudinal section  $v = 200$

ORIGINAL PAGE IS  
OF POOR QUALITY

8.4 Eutectic crystallization of the AlSi 12.5 alloy

/60

Cooling 94°C/min

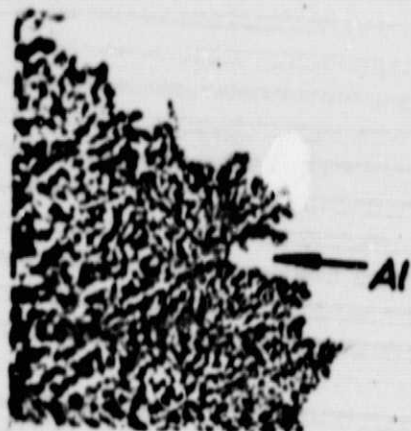


Photo 8.41: T = 573°C V = 320

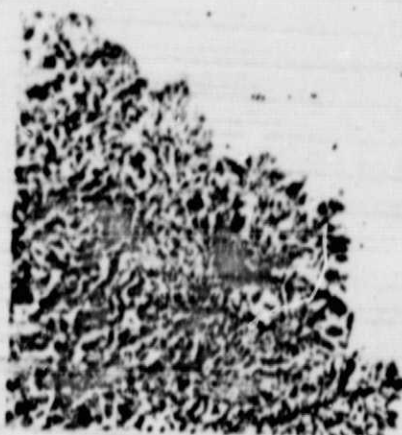


Photo 8.42: T = 573°C V = 320



Photo 8.43: T = 573°C V = 320

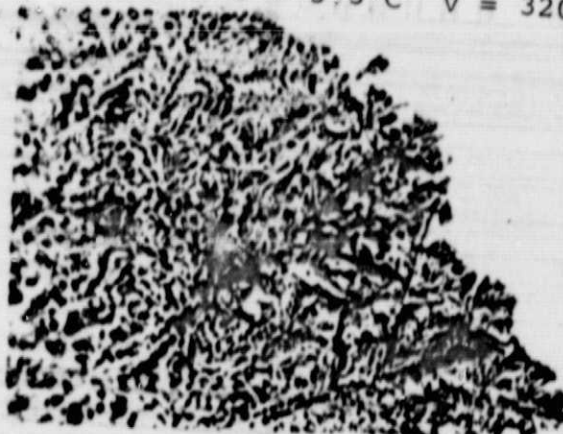


Photo 8.44: T = 573°C V = 320



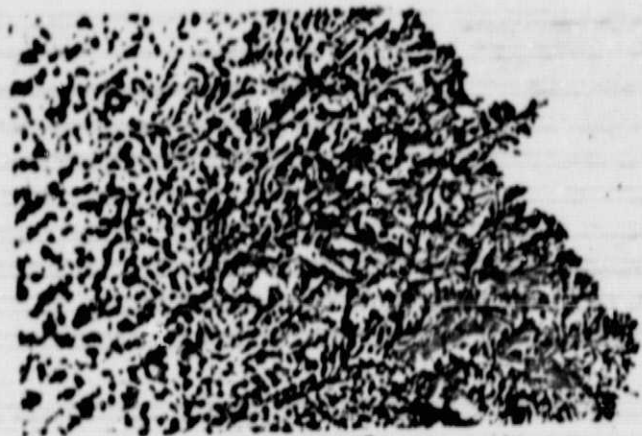


Photo 8.45: T = 573°C V = 320

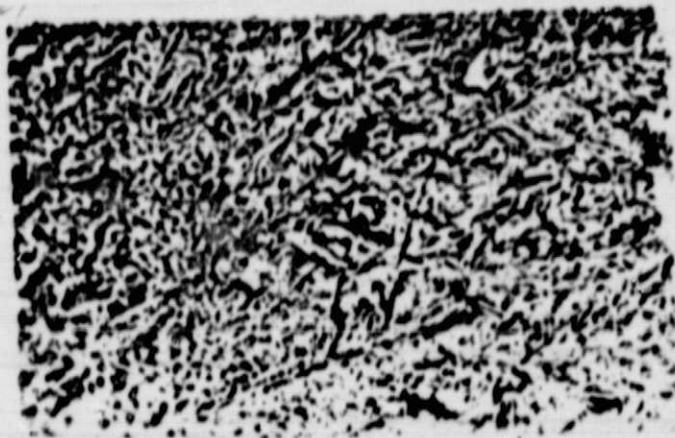


Photo 8.46: T = 573°C V = 320



Photo 8.47: Room temperature V = 320

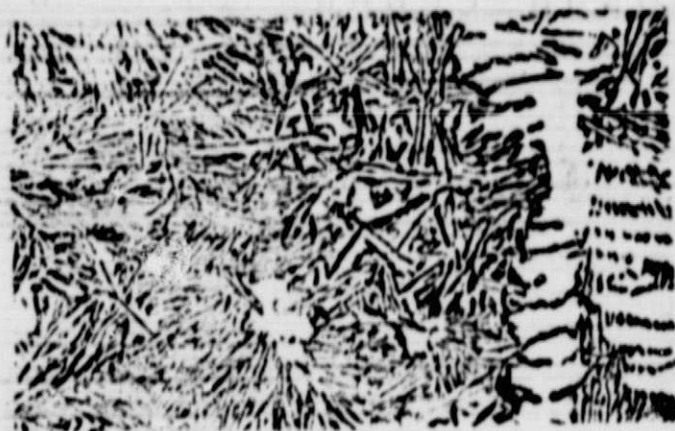


Photo 8.48: Longitudinal section V = 200

ORIGINAL PAGE IS  
OF POOR QUALITY

8.5 Crystallization of the AlSi 6 alloy without  
temperature measurement

/62



Photo 8.51: Eutectic reaction V = 320



Photo 8.52: V = 320



Photo 8.53: Room temperature V = 320



Photo 8.54: Surface cutting V = 320

8.6 Eutectic crystallization of the AlSi 12.5 Alloy

/63

Adding of Na-salt, cooling about 20°C/min, without temperature measurement

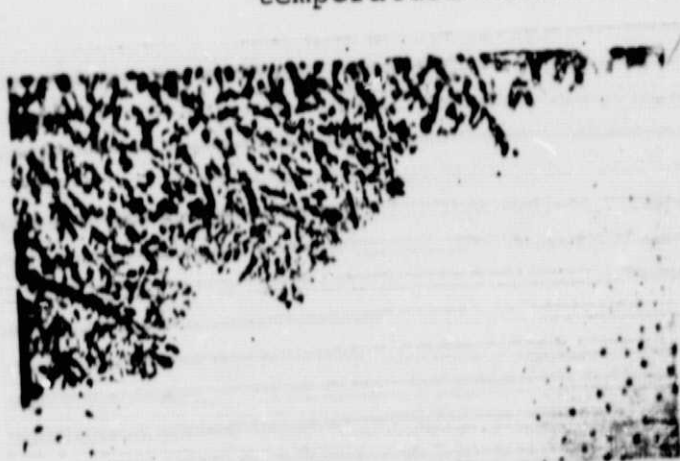


Photo 8.61: V = 320

V=320

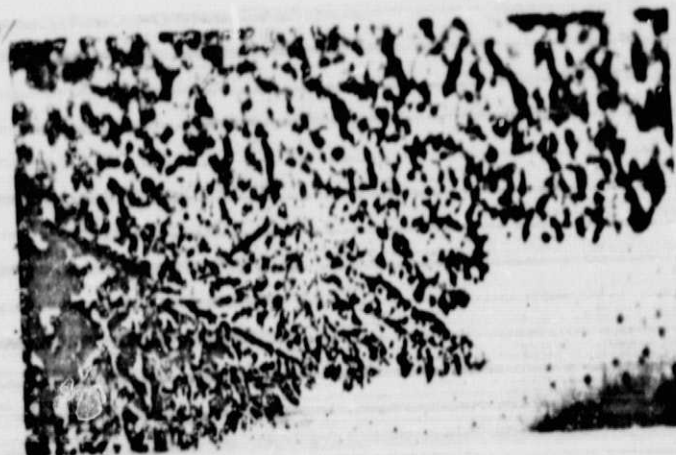


Photo 8.62: V = 320

V=320



Photo 8.63: Room temperature V = 320

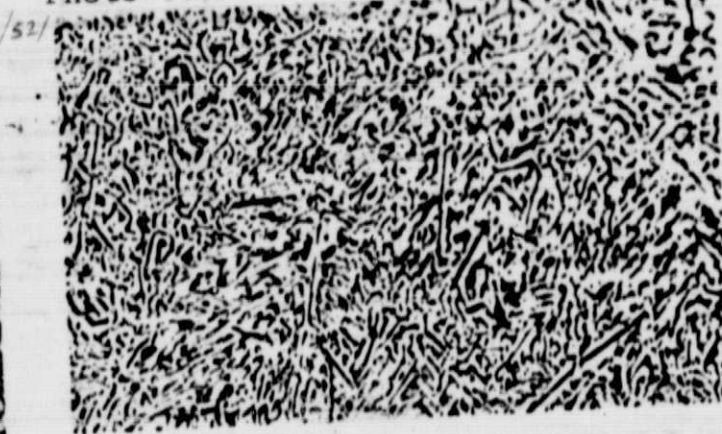


Photo 8.64: Longitudinal section V = 500

8.7 Grid scan electron microscopic photographs  
AlSi 12.5 alloy

/64



Photo 8.71:  
slowly cooled (5°C/min)  
V = 900



Photo 8.72:  
Rapidly cooled (94°C/min)  
V = 900



Photo 8.73:  
Na-enriched  
V = 900





Photo 8.74:  
Na-enriched  
V = 9000



Photo 8.75:  
cooling in water  
V = 9000



Photo 8.76:  
cooling through  
shockwave  
V = 9000



ORIGINAL PAGE IS  
OF POOR QUALITY

8.8 Eutectic crystallization of the AgSi 3.6 Alloy

/66



Photo 8.81: T = 855°C V = 320



Photo 8.82: T = 855°C V = 320



Photo 8.83: Room temperature V = 320

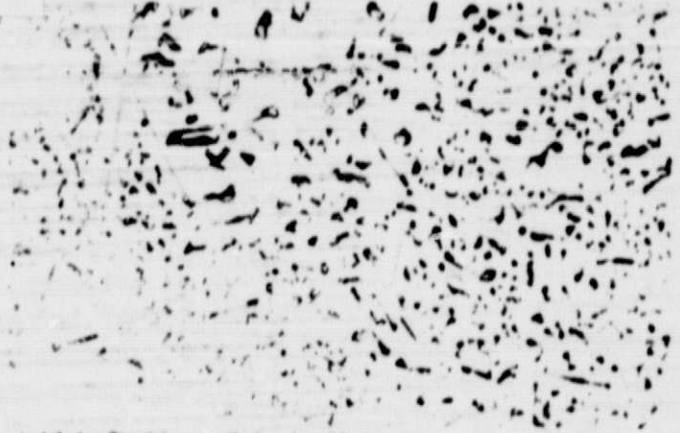


Photo 8.84: Longitudinal section  
V = 500

8.9 Eutectic crystallization of the AuSi 4 alloy

/67

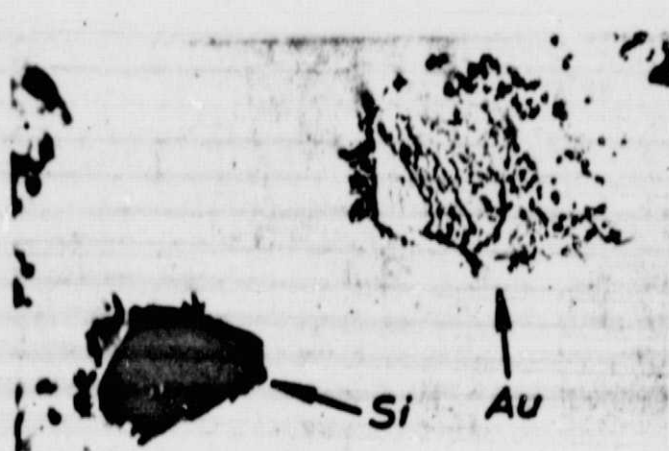


Photo 8.91: T = 370°C v = 320



Photo 8.92: T = 370°C v = 320

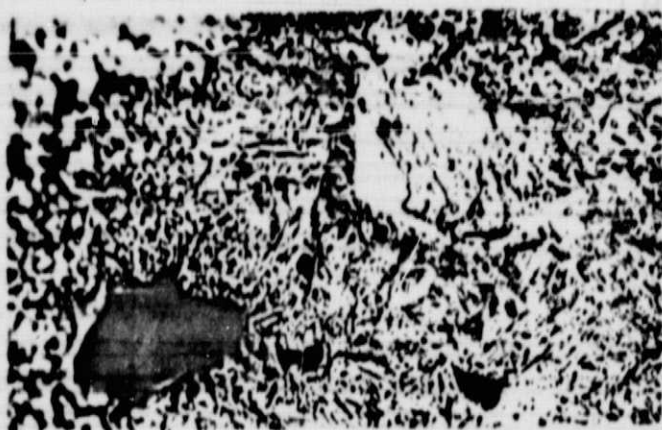


Photo 8.93: Room temperature v = 320

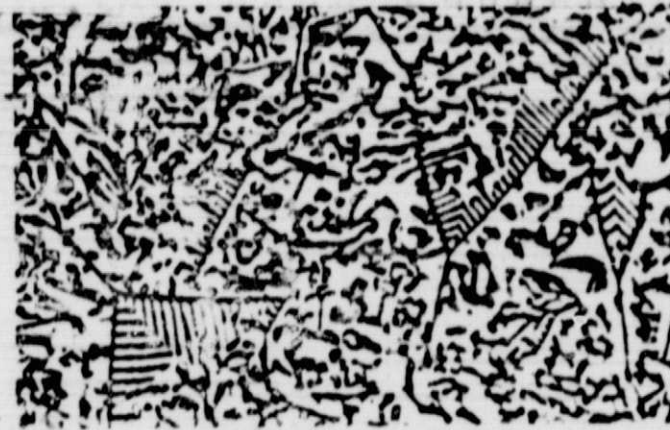


Photo 8.94: Longitudinal section  
v = 1000

## REFERENCES

- 1) K. Loehberg. Casting 44 (1957), p 89
- 2) K. Koerber. Dissertation Techn. Universitaet Berlin (Dissertation Technical University of Berlin) (D83), 1971
- 3) P. Oberhoffer. Metallurgy 6 (1909), p 554
- 4) G. Reinacher. Handbuch d. Mikroskopie i.d. Technik (Handbook of Microscopy in Technology), Vol. I, part 2, p 386, Umschau Publishing House, Frankfurt, 1969
- 5) R. Mitsche, P. Gabler and P. Juglitsch. Handbuch d. Mikroskopie i.d. Technik (Handbook of Microscopy in Technology) Vol. III, part 2, p 269, Umschau Publishing House, Frankfurt, 1969
- 6) M. G. Lozinskij. High Temperature Metallography, Pergamon Press, London, 1961
- 7) W. D. Schneider. Dissertation Technical University of Berlin (D83), 1969
- 8) D. Kossel and R. Anschutz. Leitz-Reports, Vol. II, No. 5, p 129, 1963
- 9) G. Brinson and A. J. W. Moore. J. Inst. Met. 79 (1950/51), p 429
- 10) P. J. E. Forsyth. Rev. Met. 51 (1954), p 326
- 11) B. W. Mott and S. D. Ford. Research 6 (1953), p 396
- 12) G. Reinacher. Z. Metallkunde 51 (1960), p 18
- 13) D. Altenpohl. Z. Metallkunde 46 (1955), p 535
- 14) R. Robin. Bull. Soc. d. Encouragement Ind. Nat. 18 (1912), p 204
- 15) B. A. Rogers and L. R. van Wert. Metal Progress 23 (1933) p 46 /69
- 16) P. J. E. Forsyth. Bulletin Inst. Met. 1 (1951-52), p 150
- 17) G. Reinacher. Metallographische Untersuchungen mit einem Vakuum-Heiztisch - Vortag auf der Hauptversammlung der Deutschen Gesellschaft fuer Metallkunde an 4.10.52 in Bad Neuenahr. (Metallographic Examinations with a new Vacuum Heating Table - Lecture at the Main Convention of the German Society for Metal Science on 4/10/52 in Bad Neuenahr)

- 18) G. Reinacher. Heizmikroskopische Bestimmung von Schmelzpunktrimima der Platin-Metalle - Vortrag auf der Hauptversammlung der Deutschen Gesellschaft fuer Metallkunde am 16.9.54 in Bad Pyrmont. (Heating Microscopic Determination of melting Point Minimums of the Platinum Metals - Lecture to the Main Convention of the German Society for Metal Science on 9/16/54 in Bad Pyrmont)
- 19) G. Reinacher. Vortrag auf den Journees Metallurgiques d'Automne de la Société Française de Metallurgie am 26.10.54 in Paris. (Lecture to the Jornees Metallurgiques d'Automne de la Société Française de Metallurgie on 10/26/54 in Paris)
- 20) G. Reinacher. Z. Metallkunde 45 (1954), p 493
- 21) G. Reinacher. Rev. Met. 54 (1957), p 321
- 22) F. Jeglitsch. Z. Aluminium 46 (1970), p 116
- 23) D. Turnbull and R. E. Cech. J. Apl. Phys. 21 (1950), p 804
- 24) R. E. Cech. Rev Sci. Instr. 21 (1950), p 747
- 25) D. Turnbull and R. E. Cech. Trans. AIME 191 (1951), p 242
- 26) P. Jeglitsch. Prakt. Metallogr. 1967, No. 2, p 53
- 27) R. Mitsche and P. Jeglitsch. Radex-Rdsch. 1963, No. 2, p 405
- 28) F. Jeglitsch. Berg- u. Huettenm. Mh. 109 (1964), No. 7, p 241 /70
- 29) R. Mitsche and F. Jeglitsch. Harterei - Techn. Mitt. 15 (1960), No. 4, p 201
- 30) H. J. T. Ellingham. Trans. Soc. chem. Inst. 63 (1944), p 125
- 31) F. D. Richardson and J. H. E. Jeffes, J. Iron Steel Inst. 160 (1948), p 261
- 32) M. Hansen and K. Anderko. Constitution of Binary Alloys, McGraw-Hill, New York, 1958, p 132
- 33) R. W. Smith. Proceedings of the Conference on "The Solidification of Metals" in Brighton, 1967. ISI Publ. No. 110, London, p 224
- 34) M. G. Day. ebenda, p 177
- 35) R. A. Meussner. The Aluminium Silicon Eutectic. Naval Research Laboratories, Wash. D.C. No. L-5331, 1959

- 36) G. Guertler. Z. Metallkunde 44 (1953), p 503
- 37) C. B. Kim and R. W. Heine. J. Inst. Met. 92 (1963/64) p 367
- 38) P. B. Crosley and L. F. Mondolfo. Mod. Castings 49 (1966)  
p 53
- 39) V. de L. Davies and J. M. West. J. Inst. Met. 92 (1963/64),  
p 175
- 40) K. Loehberg. Z. Metallkunde 45 (1954), p 656
- 41) G. A. Chadwick. Prog. Mat. 12 (1963), p 97
- 42) E. Scheil. Z. Metallkunde 45 (1954), p 298
- 43) E. Scheil. Z. Metallkunde 37 (1946), p 1
- 44) R. W. Kraft. Trans. AIME 624 (1962, p 65
- 45) V. de L. Davies. J. Inst. Met. 93 (1964/65), p 10
- 46) J. D. Hunt and K. A. Jackson. Trans. AIME 236 (1966), p 843
- 47) J. A. E. Bell and W. C. Winegard. J. Inst. Met. 93 (1965),  
p 318
- 48) D. J. S. Cookney, M. G. Day and A. Hellowell. International  
Conference on Crystal Growth, J. Phys. Chem. Solids (Suppl.)  
1967
- 49) M. G. Day and A. Hellowell. Proc. Roy. Soc. A 305 (1968),  
p 475
- 50) A. Hellowell. Prog. Mat. Sci. 15 (1970), Part 1
- 51) H. G. Day and A. Hellowell. J. Inst. Met. 95 (1967), p 377
- 52) P. N. Rhines and W. F. B. Timpe. Z. Metallkunde 48 (1957),  
p 109
- 53) D. D. Double and A. Hellowell. Acta Met. 17 (1969), p 1071
- 54) B. M. Thall and B. Chalmers. J. Inst. Met. 77 (1950, p 79
- 55) K. Loehberg. Techn. Mitt. 49 (1956), H.8
- 56) F. Warich and H. Winterhager. Z. Aluminium 43 (1967),  
pgs 417, 497 and 609
- 57) T. K. Imono. J. Japan Foundrymen's Soc. 41 (1969), p 434
- 58) A. Pacz. U. S. Patent 1,387,900 of Aug. 16, 1921

- 59) H. Hanemann and A. Schrader. Atlas metallographicus, Berlin 1941
- 60) E. Schulz. Z. Metallkunde 39 (1948), p 123
- 61) L. F. Mondolfo. J. Inst. Met. 73 (1950/51), p 733
- 62) E. Schultz. Z. Metallkunde 40 (1949), p 246
- 63) J. D. Edwards and R. S. Archer. Chem. Met. Eng. 31 (1924), p 504
- 64) R. S. Archer and L. W. Kempf. Trans. AIME 73 (1926), p 581
- 65) R. C. Plumb and J. E. Lewis. J. Inst. Met. 86 (1957/58) p 393
- 66) L. Tauscher. Neue Huette 10 (1965), p 743
- 67) A. G. G. Gwyer and H. W. L. Phillips. J. Inst. Met. 36 (1926), p 283
- 68) E. A. Boom. Met. Abstr. 20 (1952/53), p 81
- 69) V. de L. Davies and J. M. West. J. Inst. Met 92 (1963/64), p 175
- 70) V. de L. Davies and J. M. West. ebenda, p 208
- 71) Y. Tsumura. Nippon Kinzoku 21 (1957), p 69
- 72) S. Gosh, J. Wilcock and V. Kondic. GieBerei, Techn. Wiss. Beihefte 28 (1960), p 1575
- 73) W. J. D. Johnes and W. L. Bartlett. J. Inst. Met., 81 (1952/53), p 145
- 74) G. Akimov. Met. Prog. 49 (1946), p 973
- 75) J. A. E. Bell and W. C. Winegard. Nature 208 (1965), p 177
- 76) M. G. Day. J. Inst. Met. 98 (1970), p 57
- 77) S. Engler. Z. Aluminium 46 (1970), p 121
- 78) A. Papapetrou. Z. Kristallographie 92 (1935), p 89
- 79) K. A. Jackson, J. D. Hunt, D. R. Uhlmann and T. P. Seward. Trans. AIME 236 (1966), p 149

- 80) M. Ghoniem. Doctorate Thesis Techn. University Berlin 1967, unpublished
- 81) M. E. Glicksman and R. J. Schaefer. Proceedings of the Conference on "The Solidification of Metals" in Brighton 1967, ISI Publ. No. 110, London, p 44
- 82) Chiu Shiu-Tang. Faturwissenschaften 48 (1961), p 70
- 83) N. R. Pillai. Ph.D. Thesis, Banares Hindu University, Varanasi, India, 1971

This study was prepared at the Institute for Metal Science of the Technical University in Berlin.

At this time, I would like to thank all coworkers of the Institute who have helped in the carrying out of the examinations.

A special thanks to Professor Dr. Phil. K. Loehberg for the suggesting of this study, his helpful support as well as many helpful discussions.

I thank the German Research Society for the financial support.

Curriculum Vitae

██████████  
1947-1958 Born in ██████████  
Attendance at Primary and Secondary Schools  
in Leipzig. Graduation in Modern Languages.

1958-1960 Instructor as a Machinist in Leipzig.

1960-1961 Study at the Technical University in Dresden.

1961-1962 Attendance at a Preliminary Study Course in  
Marburg, Special Testing with Certification  
for University Studies.

1962-1968 Study at the Technical University in Berlin,  
Graduation with a Degree in Engineering in  
November, 1968.

since November 1968 Scientific Assistant at the Institute for  
Metal Science of the Technical University  
of Berlin.